Al-Rafidain Journal of Engineering Sciences

Journal homepage https://rjes.iq/index.php/rjes

ISSN 3005-3153 (Online)

Effect of Doped Aluminium into Bismuth Telluride on the Structural and Optical Properties by Thermal Evaporation

Samar S. Fazaa, Firas A. Najim

Department of Physics, College of Education, University of Al-Qadisiyah, Al-Diwaniyah, Iraq

ARTICLE INFO

Article history:
Received 16 July 2024
Revised 20 July 2024,
Accepted 07 August 2024,
Available online 08 August 2024

Keywords:
Al-doped
Bi_2Te_3 thin films
Optical properties
Structural characteristics

ABSTRACT

In this research, the structural, morphological, and optical properties of Bi2Te3 at different thicknesses (100, 200, 300 nm) and different concentrations of Al (2%, 4% and 6%) at a thickness of 100 nm for thin films. were studied that revealed the formation of the hexagonal Bi2Te3 structure for undoped and Al-doped films, XRD studies showed that the average size of the grains increased with increasing Al content from 2% to 6%, the lattice constant of the doped films was greater than the value in the international test card, the density of dislocations decreased as the Al content increased, and We also observed that the number of crystals per unit area increased with increasing thickness at (300 nm) was (0.1714 × 1010 m-3), and decreased with increasing Al content for the films at (6%) was (0.051 × 1010 m-3). EDX spectroscopy spectra demonstrated the incorporation of Al into the doped films. The optical reflectance (R%) of pure Bi2Te3 at different thicknesses, Bi2Te3/Al films, were recorded in the range of 350-840 nm. The R% were profoundly affected by Al doping. The optical bandgap decreased from 2.12 to 1.99 eV as the Al content increased from 2% to 6%. The observed optical properties of Bi2Te3/Al thin films may allow for the selection of materials with specific applications in mind, such as optical design.

1. Introduction

The investigation and development of new semiconductor properties that result in new applications and the creation of advanced and modern devices has been a topic of interest to scientists and has dedicated the majority of their research to this endeavor annually [1, 2].

Tellurium was an uncommon metal and was located in the 6th group of the Periodic table [3]. The compounds of telluride metal exhibited unique properties like high absorption capacity [4], direct band gap [5], and superior transparency in the visible region [6]. The collected samples can be utilized in solar cells [7], radiation detectors, electro-optical modulators [8], infrared sensors, optical components and lenses. Thin films were formed using various methods [9, 10].

The most effective material for room temperature use is bismuth telluride (Bi_2Te_3), which has been produced in a variety of ways, including co-evaporation [11] of 11 different chemicals, MBE [12] of 12 different chemicals, MOCVD [13, 14] of 13 different chemicals, and hydrothermal synthesis [15] of 15 different chemicals. Among this technique, the thermal evaporation method provides a high rate of deposit and a scalable approach, additionally, it is capable of adjusting multiple parameters in order to produce the desired output [16].

* Corresponding author E-mail address: phy.edu.post31@qu.edu.iq
https://doi.org/10.61268/bcbg5671

Recently, thermoelectric (TE) materials, Bi_2Te_3 and its alloys, have been found to be the most effective thermoelectric materials, their figure of merit is highest near room temperature [17].

In this research, the bismuth telluride thin films were pure at different thicknesses and were also doped with (Al) via thermal evaporation onto glass substrates. The bismuth telluride films have been characterized via various methods to study the structural, morphological, and optical properties, in order to have a comprehensive understanding of the composition, structure and properties of different thicknesses and doping by (Al) regarding the optic properties.

2. Experimental procedures

2.1 Preparation of bismuth telluride thin films pure and doping with Al

Using a high purity (99.99%) compound of (Bi_2Te_3), both pure and doped thin films were created through thermal evaporation in a vacuum. The glass substrate was thoroughly cleaned with distilled water and alcohol, then subjected to ultrasound for 15 minutes before being dried and prepared for the evaporation process. To achieve the necessary high vacuum pressure of (10^{-5} mbar), a combination of rotary pump and diffusion pump was utilized. The pressure was accurately measured using both a Pirani scale and a Penning scale. The films were deposited at a thickness of 100 nm and a rate of 0.4 nm/sec. In order to produce aluminum-doped (Al) Bi_2Te_3 films, the double evaporation (Co-Evaporation) method was employed, with varying thicknesses of 100, 200, and 300 nm inside the molybdenum bot.

To attain the desired doping weight percentages (2%, 4%, 6%) of the Bi_2Te_3 mass, we introduced aluminum material into a molybdenum bot within the vacuum chamber. Once the necessary pressure (3.5×10^{-5} mbar) was reached, we commenced the deposition process on glass substrates by gradually applying an electric current. This resulted in the simultaneous evaporation of Bi_2Te_3 and Al at varying electrode temperatures.

2.2 Characterizations and measurements

The morphologies as well as crystal structures of the thin film samples were characterized using X-ray diffraction (XRD, Rigaku D/MAX 2200 PC) with Cu Kα radiation ($\lambda = 0.154$ nm), field emission SEM and EDX to make sure of the elements in the samples and roughness was measured by an atomic force microscope (AFM). The films thickness was calculated by weight method which is not very accurate; an optical method can be used that relies on interference in thin films by rays, like a laser. Also, a UV-1800 device was used for the optical features.

3. Results and discussion

3.1 The X-ray diffraction analysis

Figure 1 (a) displays the XRD patterns of thin films, varying in thickness, that were sputtered on glass substrates. All patterns exhibit preferred crystallization diffraction at plane (015) with other planes (1010), (0111), (0210), (1115), (0216), which corresponds to [18, 19]. Observably, the peak is weak for the 100 nm thick film and this peak grows while increasing film thickness from 200 to 300 nm. Figure 1 affirms good crystallization for all films with hexagonal crystal structures; presence of secondary peak at plane (1010) confirms hexagonal crystallization and is supported by [20] information. It can be deduced from the figure that crystals' structural quality improves with thickness.

XRD patterns do affirm the structure of the films doped and deposited at 100 nm thick. No considerable shift in the peaks' diffraction was observed, confirming the existence of hexagonal phases that are with [21, 22]. The XRD patterns were found to be able to affirm the structure of doped films with 100 nm in thickness. It is noted that no significant shift in the diffraction peaks was observed. This finding confirms the presence of hexagonal phases and is in agreement with [21, 22].

3.2 Structural parameters

3.2.1 Average grain size (D)

The mean grain size for all undoped and doped bismuth telluride (Bi_2Te_3) samples was determined from the highest intensity peak in

the (015) plane. The calculation of average crystal sizes for thin films was carried out using Debye-Scherrer equation to estimate the average crystallite sizes of prepared thin film [17].

$$D = \frac{k\Lambda}{\beta cos\theta} \quad (1)$$

Where

K: represents the shape factor and its value is (0.94).

λ: X-ray wavelength (nm).

θ: diffraction angle in Braque's law.

β: is measured in radian (FWHM) (Full Width at Half Maximum).

Results revealed that the average grain size was (25.965 nm) at a thickness of (300 nm), and it increased with increasing with doping ratio to (6%) and was (26.961), as illustrated in Table 1. The increase in grain size at different doping ratios can be attributed to the fact that aluminum atoms took interstitial positions within the crystal structure, this is agreed with [23].

3.2.2 Lattice constant (a, c):

The thin films of pure bismuth telluride (Bi_2Te_3) were obtained with thickness of 100, 200, and 300 nm and the lattice constants (a, c) calculated from Equation 2, as these films belong to the hexagonal type. Aluminum-doped films were also analyzed to determine the effect of doping on the lattice constants. The values of the lattice constants [24] are:

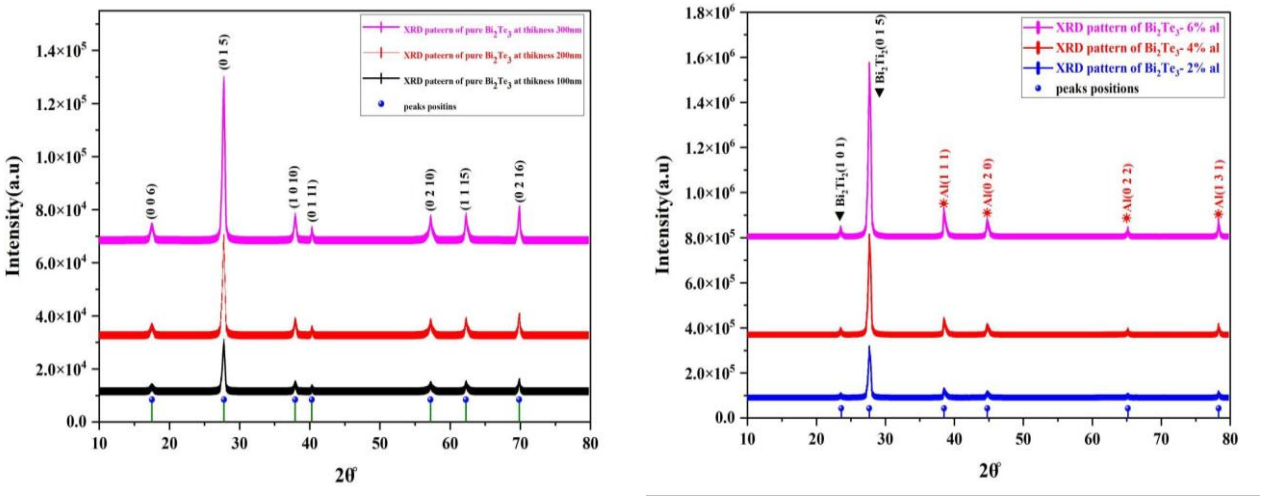

Figure 1. (a) X-Ray diffraction of Bi_2Te_3 pure at different thicknesses (100, 200, 300 nm), and (b) upon doping with varying aluminum ratios

Table (1): The results of the structural parameters of pure at different thickness (100, 200, 300 nm) (Bi_2Te_3) films, and doped with aluminum

Material	Thickness (nm)	G.S Nm	a XRD (Å°)	c XRD (A°)	a stander (Å°)	C stander (A°)	$\delta\times10^{10}$ (m^{-2})	$N°\times10^{10}$ (m^{-2})
Bi_2Te_3	100	24.056	4.4534	31.7529	4.3852	30.483	1.728	0.0718
Bi_2Te_3	200	22.999	4.4405	31.5051	4.3852	30.483	3.781	0.6144
Bi_2Te_3	300	25.965	4.3772	30.3413	4.3852	30.483	4.449	0.1714

Bi_2Te_3: Al 2%	100	21.335	4.4267	31.2454	4.3852	30.483	2.196	0.103
Bi_2Te_3: Al 4%	100	20.491	4.4506	31.699	4.3852	30.483	2.381	0.1162
Bi_2Te_3: Al 6%	100	26.961	4.4148	31.0233	4.3852	30.483	1.375	0.051

$$\frac{1}{d_{hkl}^2} = \frac{4}{3}\left(\frac{h^2 + hk + k^2}{a^2}\right) + \frac{l^2}{c^2} \qquad (2)$$

Where

d: crystal distance between planes, (h,k,l): Miller coefficients, a,b,c: represent lattice constants

Table 1 gives you an indication. The doped films have lattice constants greater than standard values in international test card and both pure and doped films behave similarly. A small increase in the lattice constant is an indication of good crystallization since deviation from original values is low, while in contrast poor crystallization would occur when deviation is high, based on [25] that's mentioned as well. We noted that aluminum doping leads to an increment in lattice constants which implies that aluminum atoms take interstitial positions within crystal structure; this observation corresponds with [26].

3.2.3 Dislocation density (δ)

The calculation of dislocation density in pure and aluminum-doped (Bi_2Te_3) thin films was done by Equation 3 as based on the grain size ratio which is inversely proportional to it.

$$\delta = \frac{1}{D_{av}^2} \qquad (3)$$

D: represents the average particle size

The observation made from Table 1 shows that the dislocation density increases with the thickness and takes a decreasing trend at (300 nm), having a value of ($4.449 \times 1010\ m^{-3}$). We also note that the dislocation density decreases with doping at (6%) which was ($1.375 \times 1010\ m^{-3}$), as well as aluminum content-dependent decrease in dislocation density, and these are in agreement with changes in stresses. Both dislocation density and lattice stress exhibit similar behavior, implying that decrease in dislocation density leads to formation of good quality films, which is supported by [27] based on changes observed in lattice constants that matches those in dislocation densities.

3.2.4 Number of crystals per unit area (N^o)

The calculation was carried out for all pure (Bi_2Te_3) films, with thickness of (100, 200, 300 nm), and doped with Al.

$$N^0 = \frac{t}{D_{av}^3} \qquad (4)$$

D: represents the average particle size

The observation made here is that the number of crystals per unit area increases with increasing thickness at (300 nm) was found to be ($0.1714 \times 1010\ m^{-3}$), and it decreases with increasing doping ratio for the films at (6%) was ($0.051 \times 1010\ m^{-3}$), as illustrated in Table 1. The decrease in the number of crystals per unit surface area is attributed to the increase in the grain size, which aligns with [28].

3.3 The SEM and EDX results

SEM images showed solid features of the structure which could impact optical properties. Figure 2 revealed that with an increase in thickness there was a rise in surface area; after Al doping into Bi_2Te_3, the morphology did not change much since the particles were all well dispersed but Bi_2Te_3/6% Al had more aggregated, denser and rougher surface which was mesoporous. Display EDX data for undoped and thickness (300 nm), doped Bi_2Te_3/6% Al thin films. Material phases identified from XRD patterns matched stoichiometric formulae from EDX analysis.

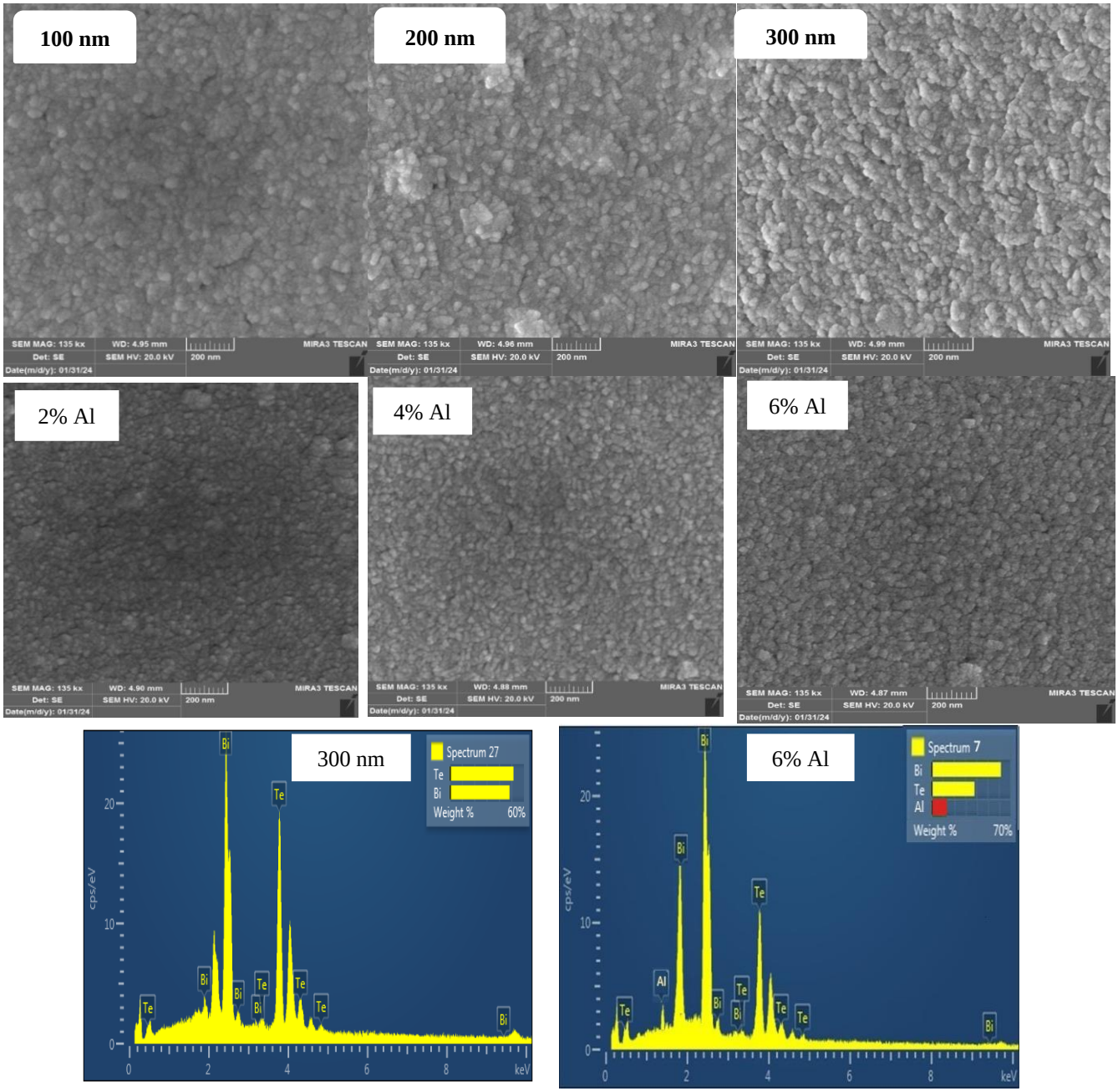

Figure 1. SEM morphology for pure thin films at different thickness and doping with Al, and EDX elemental analysis

3.4 AFM results

The AFM images of samples (Figure 3) showed an increment in the grain size and increase in the roughness of the film at increases thickness of thin films. The AFM images of the films doped with different ratio for Al revealed an increase in grain size and roughness with increase in the of ratio. AFM confirmed increase in the grain size with increase in the thickness and doping.

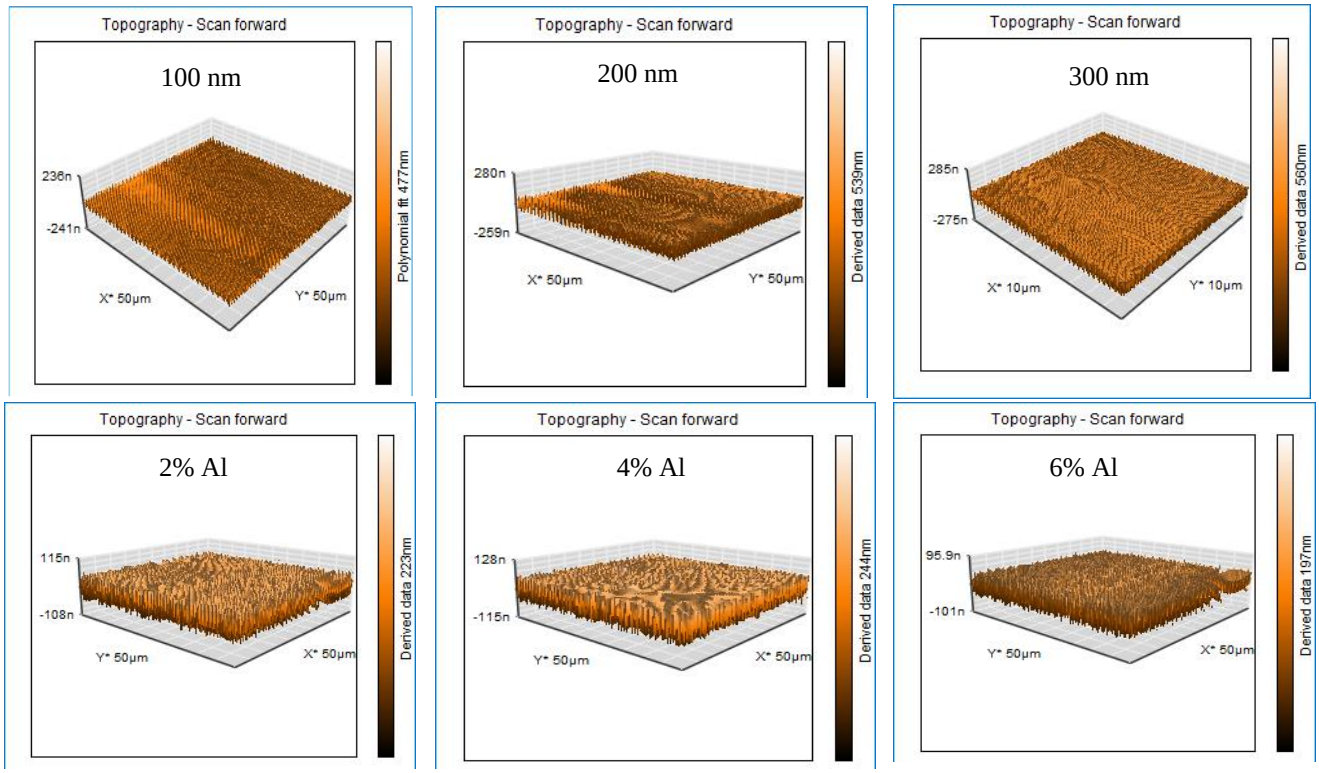

Figure 3. AFM dimensional distribution of thin films. These thin films were synthesized with various thickness and doped with different ratios of Al at a thickness of 100 nm

3.5 Optical properties

Figure 4 demonstrates the optical reflectance (R%) for Bi_2Te_3 pure with different thicknesses and Bi_2Te_3/Al doped thin films as a function of wavelength. It can be observed that, over the entire ultraviolet and visible spectral ranges, the reflectance is higher for thicker films. The values of reflectance are relatively high in the near-infrared range as well. However, overall, the reflectance decreases with Al doping, which is a behavior typical in metal-doped semiconductors as reported by previous studies [29-31]. The introduction of Al into the system enhanced the grain sizes within the films. This improvement in grain sizes hints at better crystallinity since there is now less impeding reflectance due to this phenomenon factors like grain boundaries. Therefore, reducing light scattering which leads to an increase in.

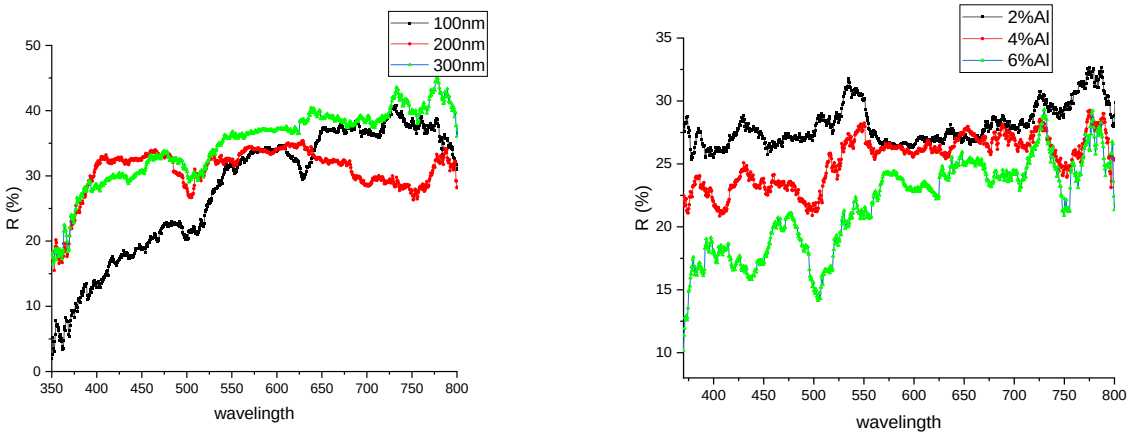

Figure 4. The pure thin films Bi_2Te_3 at different thickness show optical reflectance (R%) and also different doping Al with thickness (100 nm) is shown as a function of wavelength

3.6 The optical bandgap (Eg):

Room temperature is where the spectrum of diffuse reflection has been recorded for the bismuth telluride nanofibers that were synthesized, as shown in Figure 4. It was later converted to an absorption spectrum using the Kubelka-Munk theory [32] which is derived from Equation 5:

$$F(R) = \alpha = \frac{(1-R)^2}{2R} \quad (5)$$

Where α denotes the absorption coefficient, R stands for the diffuse reflection factor and $F(R)$ represents the Kubelka-Munk function. The optical band gap of Bi_2Te_3 thin films was determined using Tauc's law [33] which is based on different thicknesses and different doping with Al for a thickness of 100 nm; after having obtained the optical absorption coefficient calculated through Kubelka–Munk theory:

$$[F(R)h\upsilon]^n = \beta(h\upsilon - E_g) \quad (6)$$

Consequently, the defect states density is increased and the structural properties are modified by doping with Al, thus reducing the optical bandgap [29].

Extrapolation of the linear portion of $[F(R)h\upsilon]^2$ and $[F(R)h\upsilon]^{1/2}$ against $h\upsilon$ gives the corresponding optical energy gap (Eg) value, as shown in Figure 5, 6. The Eg value of Bi_2Te_3 with thickness 100 nm is 2.44 eV, 2.24 eV, while for Bi_2Te_3/6% Al it is 2.12 eV, 1.99 eV, showing that Eg can take any value from either mechanism: direct or indirect transition, indicating co-existence. Hence, by increasing the defect states density and changing structural properties, Al doping decreases the optical bandgap [29].

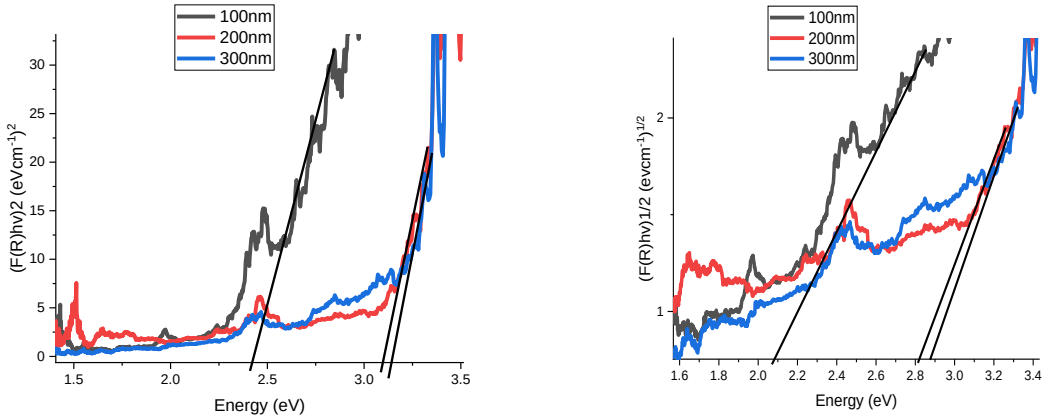

Figure 2. Energy gap $[F(R)h\upsilon]^2$ and $[F(R)h\upsilon]^{1/2}$ of the synthesized Bi_2Te_3 at different thickness

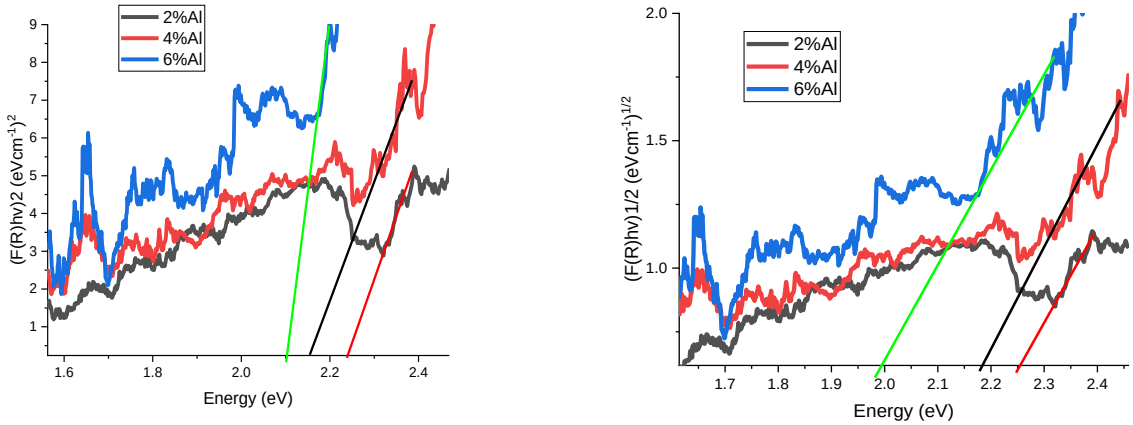

Figure 6. The Energy gap $[F(R)h\upsilon]^2$ and $[F(R)h\upsilon]^{1/2}$ of the fabricated thin films of Bi_2Te_3 implanted with Al at a thickness of (100 nm)

4. Conclusions

Bi_2Te_3 thin films were developed with different thicknesses and varied Al doping (2%, 4%, 6%) through thermal evaporation technique. XRD exposed the polycrystalline behavior of all prepared films having hexagonal structure identified. The average grain sizes were observed to be increased when doped with Al. Reflectance is directly proportional to the thickness whereas inversely proportional with the Al doping, Eg values decreased from 2.25 to 2.1 eV as the Al ratio increased from 2% to 6%.

References

[1] H. He, Z. Yang, Y. Xu, A. T. Smith, G. Yang, and L. Sun, "Perovskite oxides as transparent semiconductors: a review," Nano Convergence, vol. 7, pp. 1-10, 2020.

[2] S. Li et al., "Transparent-conductive-oxide-free front contacts for high-efficiency silicon heterojunction solar cells," Joule, vol. 5, no. 6, pp. 1535-1547, 2021.

[3] İ. A. Kariper, "Optical properties and surface energy of tellurium oxide thin film," Journal of Optics, vol. 47, pp. 504-510, 2018.

[4] K. Vu, S. Farahani, and S. Madden, "980nm pumped erbium doped tellurium oxide planar rib waveguide laser and amplifier with gain in S, C and L band," Optics Express, vol. 23, no. 2, pp. 747-755, 2015.

[5] M. Sathish and B. Eraiah, "Synthesis and structural characterization of niobium doped lead-telluride glass-ceramics," IOP Conference Series: Materials Science and Engineering, vol. 73, p. 012137, 2015.

[6] S. M. Ho, "Review on metal telluride thin films," Der Pharma Chemica, vol. 7, no. 9, pp. 56-60, 2015.

[7] J. S. Ritch, T. Chivers, M. Afzaal, and P. O'Brien, "The single molecular precursor approach to metal telluride thin films: imino-bis (diisopropylphosphine tellurides) as examples," Chemical Society Reviews, vol. 36, no. 10, pp. 1622-1631, 2007.

[8] T. Maity and S. Sharma, "Effect of gamma radiation on optical and electrical properties of tellurium dioxide thin films," Bulletin of Materials Science, vol. 31, pp. 841-846, 2008.

[9] H. Kong, J.-B. Yeo, and H.-Y. Lee, "A Study on the properties of tellurium-oxide thin films based on the variable sputtering gas ratio," Journal of the Korean Physical Society, vol. 66, pp. 1744-1749, 2015.

[10] S. M. Ho, "Fabrication of Cu4SnS4 Thin Films: A Review," Engineering, Technology & Applied Science Research, vol. 10, no. 5, pp. 6161-6164, 2020.

[11] G. J. Snyder and E. S. Toberer, "Complex thermoelectric materials," Nature Materials, vol. 7, no. 2, pp. 105-114, 2008.

[12] X. Liu et al., "Structural properties of Bi2Te3 and Bi2Se3 topological insulators grown by molecular beam epitaxy on GaAs (001) substrates," Applied Physics Letters, vol. 99, no. 17, p. 171903 2011.

[13] R. Venkatasubramanian, T. Colpitts, E. Watko, M. Lamvik, and N. El-Masry, "MOCVD of Bi2Te3, Sb2Te3 and their superlattice structures for thin-film thermoelectric applications," Journal of Crystal Growth, vol. 170, no. 1-4, pp. 817-821, 1997.

[14] A. Bailini et al., "Pulsed laser deposition of Bi2Te3 thermoelectric films," Applied Surface Science, vol. 254, no. 4, pp. 1249-1254, 2007.

[15] X. Zhao, X. Ji, Y. Zhang, T. Zhu, J. Tu, and X. Zhang, "Bismuth telluride nanotubes and the effects on the thermoelectric properties of nanotube-containing nanocomposites," Applied Physics Letters, vol. 86, no. 6, p. 062111 2005.

[16] C. Boulanger, "Thermoelectric material electroplating: a historical review," Journal of Electronic Materials, vol. 39, pp. 1818-1827, 2010.

[17] S. Altindal, J. Farazin, G. Pirgholi-Givi, E. Maril, and Y. Azizian-Kalandaragh, "The effects of (Bi2Te3–Bi2O3-TeO2-PVP) interfacial film on the dielectric and electrical features of Al/p-Si (MS) Schottky barrier diodes (SBDs)," Physica B: Condensed Matter, vol. 582, p. 411958, 2020.

[18] Y. Zhang, L. Hu, T. Zhu, J. Xie, and X. Zhao, "High yield Bi2Te3 single crystal nanosheets with uniform morphology via a solvothermal synthesis," Crystal Growth and Design, vol. 13, no. 2, pp. 645-651, 2013.

[19] S. Vinoth et al., "Bi2Te3 thin hexagonal nanoplatelets: Synthesis and its characterization studies," Physica E: Low-Dimensional Systems and Nanostructures, vol. 92, pp. 17-22, 2017.

[20] L. Yang, Z.-G. Chen, M. Hong, G. Han, and J. Zou, "Enhanced thermoelectric performance of nanostructured Bi2Te3 through significant phonon scattering," ACS Applied Materials and Interfaces, vol. 7, no. 42, pp. 23694-23699, 2015.

[21] B. Jariwala, D. Shah, and N. Ravindra, "Influence of doping on structural and optical properties of Bi2Te3 thin films," Thin Solid Films, vol. 589, pp. 396-402, 2015.

[22] P. Kumar, K. Sandeep, V. S. Kindalkar, A. Kote, and S. Dharmaprakash, "Non-polar a-plane oriented ZnO: Al thin films for optoelectronic applications," Physica B: Condensed Matter, vol. 606, p. 412721, 2021.

[23] S. Elahi, A. Taghizadeh, A. Hadizadeh, and L. Dejam, "Effect of thickness and annealing on structural and optical properties of Bi2Te3 thin films prepared from Bi2Te3 nanoparticels," International Journal of Thin Films Science and Technology, vol. 3, no. 1, pp. 13-18, 2014.

[24] M. N. Harif et al., "An approach to alternative post-deposition treatment in CdTe thin films for solar cell application," Superlattices and Microstructures, vol. 147, p. 106687, 2020.

[25] S. Cho, Y. Kim, A. DiVenere, G. K. Wong, J. B. Ketterson, and J. R. Meyer, "Antisite defects of Bi 2 Te 3 thin films," Applied Physics Letters, vol. 75, no. 10, pp. 1401-1403, 1999.

[26] H.-P. Cheng et al., "Effects of substrate temperature on nanomechanical properties of pulsed laser deposited Bi2Te3 films," Coatings, vol. 12, no. 6, p. 871, 2022.

[27] R. Sathyamoorthy and J. Dheepa, "Structural characterization of thermally evaporated Bi2Te3 thin films," Journal of Physics and Chemistry of Solids, vol. 68, no. 1, pp. 111-117, 2007.

[28] R. Sathyamoorthy, S. K. Narayandass, and D. Mangalaraj, "Effect of substrate temperature on the structure and optical properties of CdTe thin film," Solar Energy Materials and Solar Cells, vol. 76, no. 3, pp. 339-346, 2003.

[29] P. Priyadarshini, S. Das, and R. Naik, "A review on metal-doped chalcogenide films and their effect on various optoelectronic properties for different applications," RSC Advances, vol. 12, no. 16, pp. 9599-9620, 2022.

[30] S. Mohamed, "Photocatalytic, optical and electrical properties of copper-doped zinc sulfide thin films," Journal of Physics D: Applied Physics, vol. 43, no. 3, p. 035406, 2010.

[31] M. S. Alqahtani, N. Hadia, S. Mohamed, and M. Awad, "Effect of Fe doping on the structural, electrical and optical properties of Bi2Te3 thin films," Bulletin of Materials Science, vol. 46, p. 11, 2023.

[32] C. Karunakaran, S. S. Raadha, and P. Gomathisankar, "Microstructures and optical, electrical and photocatalytic properties of sonochemically and hydrothermally synthesized SnO2 nanoparticles," Journal of Alloys and Compounds, vol. 549, pp. 269-275, 2013.

[33] G. Saffarini, J. Saiter, and H. Schmitt, "The composition dependence of the optical band gap in Ge–Se–In thin films," Optical Materials, vol. 29, no. 9, pp. 1143-1147, 2007.